1-1-2011

Novel folding and stability defects cause a deficiency of human glutathione transferase omega 1

Huina Zhou
Australian National University

Joseph Brock
Australian National University

Marco G. Casarotto
Australian National University

Aaron J. Oakley
Australian National University, aarono@uow.edu.au

Philip G. Board
Australian National University

Novel folding and stability defects cause a deficiency of human glutathione transferase omega 1

Abstract

The polymorphic deletion of Glu-155 from human glutathione transferase omega1 (GSTO1-1) occurs in most populations. Although the recombinant ΔGlu-155 enzyme expressed in Escherichia coli is active, the deletion causes a deficiency of the active enzyme in vivo. The crystal structure and the folding/unfolding kinetics of the ΔGlu-155 variant were determined in order to investigate the cause of the rapid loss of the enzyme in human cells. The crystal structure revealed altered packing around the Glu-155 deletion, an increase in the predicted solvent-accessible area and a corresponding reduction in the buried surface area. This increase in solvent accessibility was consistent with an elevated Stern-Volmer constant. The unfolding of both the wild type and ΔGlu-155 enzyme in urea is best described by a three-state model, and there is evidence for the more pronounced population of an intermediate state by the ΔGlu-155 enzymes. Studies using intrinsic fluorescence revealed a free energy change around 14.4 kcal/mol for the wild type compared with around 8.6 kcal/mol for the ΔGlu-155 variant, which indicates a decrease in stability associated with the Glu-155 deletion. Urea induced unfolding of the wild type GSTO1-1 was reversible through an initial fast phase followed by a second slow phase. In contrast, the ΔGlu-155 variant lacks the slow phase, indicating a refolding defect. It is possible that in some conditions in vivo, the increased solvent-accessible area and the low stability of the ΔGlu-155 variant may promote its unfolding, whereas the refolding defect limits its refolding, resulting in GSTO1-1 deficiency.

Disciplines

Life Sciences | Physical Sciences and Mathematics | Social and Behavioral Sciences

Publication Details

Zhou, H., Brock, J., Casarotto, M. G., Oakley, A. J. & Board, P. G. (2011). Novel folding and stability defects cause a deficiency of human glutathione transferase omega 1. Journal of Biological Chemistry, 286 (6), 4271-4279.

Novel folding and stability defects cause a deficiency of human glutathione transferase Omega 1.

Huina Zhou†, Joseph Brock*, Marco G. Casarotto†, Aaron J Oakley* and Philip G Board†‡

† John Curtin School of Medical Research, Australian National University, Canberra ACT 2601 Australia; *Research School of Chemistry, Australian National University, Canberra ACT 2601 Australia.

‡ Correspondence to Prof Philip Board, John Curtin School of Medical Research Australian National University, PO Box 334 Canberra, ACT 2601 Australia

Tel 61 2 61254714

Fax 61 2 61254712

Email Philip.Board@anu.edu.au

Running title: Structure of GSTO1-1 ΔE155.

Key words: Glutathione transferase Omega, GSTO1-1 deficiency, crystal structure, protein folding,

Synopsis

The polymorphic deletion of E155 from human GSTO1-1 occurs in most populations. Although the recombinant ΔE155 enzyme expressed in *E. coli* is active, the deletion causes a deficiency of the active enzyme *in vivo*. The crystal structure and the folding/unfolding kinetics of the ΔE155 variant were determined in order to investigate the rapid loss of the enzyme in mammalian cells. The crystal structure revealed altered packing around the E155 deletion, an increase in the predicted solvent accessible area and a corresponding reduction in the buried surface area. This increase in solvent accessibility was consistent with an elevated Stern-Volmer constant. The unfolding of both the wild type and ΔE155 enzymes in urea is best described by a three state model, and there is evidence for the more pronounced population of an intermediate state in the ΔE155 enzymes. Studies using intrinsic fluorescence revealed a free energy change around 14.4 kcal/mol for the wild type compared with around 8.6 kcal/mol for the ΔE155 variant, which indicated a decrease in stability associated the with E155 deletion. Urea induced unfolding of the wild type GSTO1-1 was reversible through an initial fast phase followed by a second slow phase. In contrast the ΔE155 variant lacks the slow phase, indicating a refolding defect. It is possible that in some conditions *in vivo*, the increased solvent accessible area and the low stability of the ΔE155 variant may promote its unfolding while the refolding defect limits its refolding, resulting in GSTO1-1 deficiency.

Introduction

The Omega class glutathione transferases (GSTO) are among the more recently identified members of the cytosolic glutathione transferase super family (Board et al., 2000, Whitbread et al., 2003). Members of the Omega class have a number of novel features and have been implicated in important metabolic pathways and in the aetiology of some common neurological diseases (Whitbread et al., 2005, Zakharyan et al., 2001, Li et al., 2002, Li et al., 2006, Kolsch et al., 2007). In contrast to the other human GSTs, that have active site tyrosine or serine residues, the Omega class GSTs have an active site cysteine residue that is essential for its primary catalytic activities (Board et al., 2000). The Omega class GSTs were originally shown to catalyse thioltransferase and ascorbate reductase reactions and other studies have shown that they also catalyse the reduction of monomethylarsonate (MMA), in the methylation pathway for the disposition of arsenic (Whitbread et al., 2005, Zakharyan et al., 2001). In addition, recent studies have shown that GSTO1-1 has *S*-phenacyl glutathione reductase activity and plays a significant role in the biotransformation of α-haloketones (Board and Anders, 2007, Board et al., 2008). As well as these catalytic activities, GSTO1-1 has been implicated in the post-translational processing and activation of the proinflammatory mediator interleukin-1β (IL-1β) (Laliberte et al., 2003) and has also been found to act as an inhibitor of cardiac muscle ryanodine receptor Ca^{2+} channels (Dulhunty et al., 2001). Interestingly, some genetic mapping studies have strongly implicated an Omega class GST as a factor influencing the age at onset of Alzheimer' and Parkinson" diseases (Li et al., 2002, Li et al., 2003, Li et al., 2006). Other studies have implicated genetic variation in *GSTO1* in vascular dementia, stroke and cerebrovascular atherosclerosis (Kolsch et al., 2004, Kolsch et al., 2007). The mechanism by which genetic variation mediates these effects has not been determined but it could be via effects on the activity or expression of the Omega class GSTs.

Previous studies have identified a range of polymorphisms in the GSTO genes (Whitbread et al., 2003, Whitbread et al., 2005, Paiva et al., 2008). While a number of single nucleotide polymorphisms have been identified in non-coding regions, their effects on transcription, splicing and mRNA stability have yet to be evaluated (Mukherjee et al., 2006). In contrast several polymorphisms in coding regions have been studied in more detail (Whitbread et al., 2003, Whitbread et al., 2005, Paiva et al., 2008, Tanaka-Kagawa et al., 2003). A polymorphic deletion of three base pairs at the junction of exon 4 and intron 4 is of particular interest. This deletion could result in the deletion of Glu155 or a splicing abnormality. This polymorphism has been identified in a range of different ethnic groups reaching a frequency of over 10% in one Chinese sample (Whitbread et al., 2003, Yu et al., 2003, Marnell et al., 2003, Paiva et al., 2008, Schmuck et al., 2005). The deletion occurs in two haplotypes characterized by a Glu or Lys at position 208 (Schmuck et al., 2005). Recombinant expression of the Glu155 deletion variant in *E.coli* affords an active enzyme that has decreased heat stability (Whitbread et al., 2003, Schmuck et al., 2005). We recently reported that the T-47D breast cancer cell line is hemizygous for the Glu155 deletion allele and is deficient in GSTO1-1 enzymatic activity (Schmuck et al., 2008). In addition, lymphoblastoid cell lines from individuals who were heterozygous for the Glu155 deletion were reported to have only 50 % of normal catalytic activity with 4-nitrophenacylglutathione (4NPG), a specific GSTO1-1 substrate (Schmuck et al., 2008). These studies suggest that the Glu155 deletion variant is very compromised *in vivo*.

Given the role played by GSTO1-1 in the disposition of α-haloketones (Board and Anders, 2007) and the targeting of GSTO1-1 by anti-inflammatory drugs (Laliberte et al., 2003) as well as the proposed role of genetic variation in *GSTO1* in the progress of several neurological disorders (Li et al., 2006, Kolsch et al., 2007), it is apparent that natural polymorphisms in *GSTO1* that affect function are of significant pharmacogenetic and clinical interest. Consequently we have investigated the effect of the polymorphic Glu155 deletion on the enzyme's structure and stability by solving its crystal structure and studying its unfolding equilibrium.

Methods

Expression of recombinant GSTO1-1 variants.

In this study several recombinant GSTO1-1 isoenzymes have been studied. There is a common polymorphism where Asp140 substitutes Ala140. This substitution does not appear to influence function but since Ala140 is the most common allele we refer to it as the wild type and the substituted variant as A140D. In each case the Glu155 deletion variants have alanine at residue 140. cDNAs encoding GSTO1-wild type, GSTO1-A140D, GSTO1 ΔE155/E208 and GSTO1 ΔE155/K208 were cloned into the pHUE expression vector and transfected into *E. coli* BL21(DE3). The expression and purification of recombinant proteins using the pHUE vector and ubiquitin cleavage techniques have been previously described in detail (Baker et al., 2005). Briefly, the recombinant 6xHis-Ubiquitin-GSTO fusion protein was purified by chromatography on Ni-agarose. The His-Ubiquitin fusion moiety was removed by digestion with the catalytic core of Usp2, and re-chromatography on Ni-agarose. The purified proteins were dialysed against 20 mM Tris pH8, 60 mM NaCl, 5 mM dithiothreitol for storage and crystallization experiments.

Crystallization and structural determination of GSTO1-1 ΔE155/E208.

Unsuccessful attempts were made to grow crystals of GSTO1 ΔE155 under identical conditions to those reported for the native enzyme (Board et al., 2000). The protein was therefore subjected to the Index screen (Hampton Research) to find new conditions. The vapour diffusion technique was employed using a 96 well, sitting drop crystallization tray (Nunc, Roskilde, Denmark). For screening, 1 μL of protein (12 mg/ml) was mixed with 1 μL of 10mM glutathione and 1 μL of reservoir solution. Reservoirs contained 100 μl of each screen condition. The tray was then sealed with Crystal Clear tape (Hampton Research) and allowed to equilibrate at 18° C. After 6 days, crystals were observed in condition 62 (0.1 M Tris pH 8.5, 0.2 M trimethyl amine N-oxide dihydrate, 20 % (w/v) polyethylene glycol monomethyl ether 2000). Scaling up was achieved via a doubling of the overall crystallisation volume using the same method. Crystals were flash frozen at 100K using an Oxford cryostream. Cryoprotection was by sequential transfer to artificial mother liquor containing 20 % glycerol by 5 % increments. The crystals were then transferred to liquid nitrogen and stored until subsequent data collection using a Rigaku RU-200 rotating anode X-ray generator with mirror optics and Mar345 desktop beamline. Processing of data collected from a single crystal was performed using the programs DENZO and SCALEPACK (Otwinowski and Minor, 1997). Phase information was obtained by molecular replacement using the structure of the native enzyme (Board et al., 2000) as a search model with the program MOLREP (Vagin and Teplyakov, 1997). Model rebuilding to match experimental density, including the deletion of E155, was achieved with the programs O (Jones et al., 1991) and Coot (Emsley and Cowtan, 2004) and alternated with restrained refinement by the program REFMAC (Murshudov et al., 1997). The program PHENIX (Adams et al., 2002) was then employed for the final stages of refinement using the simulated annealing option with default settings. Finally, the program MolProbity (Davis et al., 2007) was used to add hydrogens to the structure and diagnose Asn/Gln/His flips prior to validation deposition, PDB accession code 3LFL.

Spectroscopy and activity measurements

All fluorescence data were measured on Perkin-Elmer LS 50B Luminescence Spectrophotometer (Perkin Elmer, USA). Tryptophan fluorescence was used to monitor structural change. Excitation was at 295 nm and fluorescence was recorded in the range of 305 nm – 430 nm. ANS (1-anilino-8-naphthalene sulfonate) was added to protein samples in a molar ratio of 50:1 (Erhardt and Dirr, 1995), and equilibrated for 50 min for complete interaction. ANS binding spectra were recorded in the range of 405 nm – 540 nm with excitation at 390nm. Enzymatic activity was determined with the GSTO1-1 specific substrate *S*-(4-nitrophenacyl)-glutathione (4NPG) as described previously (Board et al., 2008).

Tryptophan fluorescence quenching by acrylamide

Acrylamide (8M) was added to 1uM GSTO1 proteins (calculated by a molar extinction coefficient of 82800 $M^{-1}cm^{-1}$ at 280nm) to achieve different concentrations, and mixed thoroughly. Fluorescence intensities were monitored at 336 nm. Each protein sample was repeated at least 3 times, and then averaged. Quenching data were analyzed by the Stern-Volmer equation (Lakowicz, 1986):

$$\frac{F_o}{F} - 1 = K_{sv}[Q] \quad (1)$$

where F_o and F are the fluorescence intensities before and after the addition of acrylamide. $[Q]$ is the acrylamide concentration, and K_{SV} is the Stern-Volmer constant, which can reflect the burial of tryptophan residues and thus indicate the protein accessibility.

Circular dichroism measurement

Circular dichroism (CD) was monitored on Chirascan™ Circular Dichroism Spectrometer (Applied Photophysics) using a cuvette with a 0.1cm light path. Ellipticity at 222nm was collected and plotted against variation of urea concentration.

Equilibrium unfolding experiments

Urea-induced unfolding experiments were performed in 20 mM sodium dihydrogen phosphate with 40mM ammonium phosphate, pH 7.0, at 1 μM protein concentration. To reach equilibrium, protein samples with different urea concentrations (0-9 M) were incubated at 30° C for 5 hours, and then cooled down to room temperature for intrinsic fluorescence, ANS binding, and circular dichroism measurements. For the analysis of the intrinsic fluorescence the ratio of emission intensity at 333 nm (folded protein) and 355 nm (unfolded protein) was determined, and the relative intensity at 475 nm was determined for ANS binding. Data from 3-4 separate replicates from two purification batches of each protein were averaged.

Urea unfolding curves were fitted to a two-state ($N_2 \leftrightarrow 2U$) unfolding model or a three-state model ($N_2 \leftrightarrow I \leftrightarrow 2U$)(Szpikowska and Mas, 1996, Gloss and Matthews, 1997)using SigmaPlot version 10.0, and the equilibrium fractions of native, intermediate, and denatured state were solved (Gloss and Matthews, 1997) .

Protein refolding

Refolding of unfolded proteins was detected using 4NPG reduction assay and tryptophan fluorescence recovery. For activity reversibility, proteins were brought to a concentration of 1 μM in 6 M urea and allowed to unfold for 5hrs at 30° C. The proteins were then diluted 6 times, and allowed to refold at room temperature. Enzyme activity was determined after 1hr. When refolding was monitored by intrinsic

fluorescence, 30uM proteins were fully unfolded in 7.4 M urea. The enzymes were then diluted 10 times, and the emission intensities were recorded every minute.

Results

Crystal structure of GSTO1 ΔE155/K208

To determine whether the deletion of E155 caused any significant structural alterations, we crystallized and solved the structure of the GSTO1 ΔE155/E208 variant. The crystals were found to be of a different space group ($P2_12_12$) compared with the native enzyme ($P3_121$) and diffracted to 2.1 Å. Table 1 summarizes the crystallographic data and model statistics.

Molecular replacement in MOLREP (Vagin and Teplyakov, 1997) revealed 3 monomers in the asymmetric unit. Monomer A sits adjacent to a crystallographic two-fold axis so as to form a physiological dimer with its crystallographic partner (A-A). Monomers B and C form a second dimer (B-C). The overall topology is similar to that of the wild-type enzyme, except for the following: the deletion of residue E155 results in the premature termination of helix α5 and a conformational change in the helix α5 to α6 loop (Figure 1A). Its subsequent removal from the search model required significant rebuilding of the associated residues, a process coupled with restrained refinement until local aberrations in the mF_o-DF_c electron density map were removed. As shown in figure 1B, several perturbations in the surrounding structure contribute to this enzyme's altered phenotype. The hydrophobic interactions (not shown in this figure) of adjacent residues Val156 and Leu157 have been disrupted by Cα translations of 5.3 Å and 8.0 Å, respectively. This has caused Val156 to be exposed to solvent. The translocation of Leu157 on the other hand, has produced a new interaction with Leu119 and of particular interest, an interaction with the side chain of Pro68 from the other subunit in the physiological dimer, effectively creating a new interaction at dimer interface. In addition, the Thr158 Cα has shifted by 6.4 Å, allowing its side chain to occupy the position previously inhabited by that of Val156. Such changes have contributed to an increase in the water accessibility of Leu157 to over 100 $Å^2$ and an increase in the buried area at the interface of twice this magnitude. In total there are only 7 contacts ≤ 3.5 Å between residues 150-164 of α5 and residues 192-202 of loop-α7 in the ΔE155/E208 enzyme, 18 fewer than in the wild type enzyme. The altered packing has likely played a role in the observed refolding anomaly of E155 deletion variants discussed below. The alterations in the dimer interface do not appear to preclude the formation of heterodimers between wild type and deletion-containing monomers.

The potential flexibility of the C-terminal region can be observed in the ΔE155/E208 structure. Comparison of the active site of monomer A with the wild type enzyme reveals a rotation of the putative 'H-site' residue, Trp222, resulting in the removal of its indole nitrogen from the binding pocket, increasing its hydrophobic character. As shown in figure 2A, the entrance to the binding pocket has also been partially occluded by the movement of Arg183 and Tyr229. Helix α9, of monomer A which forms part of the active site, has shifted away from the GSH binding pocket (G-site), possibly to accommodate movements in residues Tyr229 and Trp222 (figure 2A). While the B and C monomers display similar structural changes relating to the deletion site, it is the conformational shift of their C-termini that is most remarkable. As shown in figure 2B helix α9 of monomer B has moved toward the G-site and rotated so that Leu228 and Tyr229 block the H-site entrance. There is a significant

rearrangement of Trp222, which has been excluded from the H-site and is stacked against helix α6, exposed to bulk solvent. The net effect is to make the 'H-site' smaller. Furthermore, the last 10-14 residues forming helix α10 and its connecting loop fail to show substantial $2mF_o$-DF_c density in monomers B and C. These significant changes do not appear to be a consequence of crystal packing, as the crystal contacts in each monomer are different. The different conformations seen in the two dimers (A-A and B-C) may therefore reflect the conformational space sampled in solution. Such helix α9 movements may be crucial to the binding of ligands of variable size and shape, for example mono methylarsonate and dehydroascorbate.

Equilbrium unfolding /folding of GSTO1 ΔE155/E208

Initially, to determine if the deletion of E155 caused subtle changes to the enzyme's conformation in solution, the Stern-Volmer constant (K_{SV}) was calculated by quenching the natural tryptophan fluorescence using acrylamide. Linear Stern-Volmer plots revealed a clear difference between the variant enzymes with the E155 deletion and the enzymes with A or D at residue 140 (Figure 3). This difference is reflected numerically in K_{SV} for each enzyme (5.258 (R^2 = 0.9989) for wild type (A140), 5.840 (R^2 = 0.9982) for A140D, 6.975 (R^2 = 0.999) for ΔE155/E208, and 7.299 (R^2 = 0.9979) for ΔE155/K208). The data suggest that the deletion of E155 increases the accessibility of tryptophan residues. This is supported by calculations from the crystal structure of increased accessible surface area (ASA) of total protein and of tryptophan residues in the ΔE155 (Table 2).

Characterization of urea-induced unfolding.

The unfolding of the GSTO1-1 enzymes in the presence of urea was examined using tryptophan fluorescence, circular dichroism (CD) and ANS binding (Figure 4). The fluorescence data (Figure 4a), for the wild type and A140D enzymes indicate that they do not begin unfolding before the urea concentration exceeds 3.7 M, and appear to exhibit a single transition phase. In contrast, the equilibrium denaturation of the ΔE155 enzymes start to show an unfolding signal below 1M urea, and have a biphasic transition profile. The difference in the unfolding profiles between the E155 containing and ΔE155 enzymes is also observed for the CD data (Figure 4b) where the ΔE155 enzymes start losing their helical secondary structure content at the lowest concentrations of urea. It is also of interest to note that at the starting point of the unfolding curve in Figure 4b the ΔE155 variants have a lower helical content than the wild type enzymes, which is consistent with the ΔE155/E208 structure. The data from the ANS binding measurements (Figure 4c) provides the clearest evidence that the unfolding profiles of the ΔE155 enzymes are different to the E155 containing enzymes. Using tryptophan fluorescence, protein concentration dependence was observed for the transition phase of the wild type enzyme and the second transition phase of the ΔE155/E208 enzyme (figure 5). Taken together, this data suggested that the equilibrium unfolding of the wild type and A140D enzymes might be described by a two state model ($N_2 \leftrightarrow 2U$) while the unfolding of the ΔE155 enzymes might best be described by a three state unfolding model ($N_2 \leftrightarrow I \leftrightarrow 2U$).

Tryptophan fluorescence and ANS binding data from the ΔE155 enzymes were fitted to a three state model with an R^2>0.999, while the fitting of fluorescence data from the wild type and A140D enzymes to a two state model gave a slightly lower R^2 (0.9986 and 0.9974 respectively) and lower free energy values (Table 3) that were inconsistent with the previously observed lower thermal stability for ΔE155 enzymes (Whitbread et al., 2003). When the same three state model was used to re-fit the data from the wild type and A140D enzymes, a better fit (figure 4a) with a higher R^2

(>0.9993) was obtained. Based on the fitting result (Table 3), equilibrium denaturation of the wild type and A140D proteins appears to be better described by a three state unfolding model. Given the protein concentration dependence of the transition phase of both enzymes (Figure 5) it appears that the transition intermediate formed by the ΔE155 enzymes is likely to be a dimer. It is not clear whether this is the case for wild type and A140D enzymes.

The population of the transition intermediate appears to differ significantly between the E155 containing and ΔE155 enzymes. Based on the three state model, the fractions of the transitional intermediate, and the native and unfolded states at different urea concentrations were calculated and plotted (figure 4d-4f). The population of intermediate formed by the wild type and A140D enzymes is largely overlapped by the unfolded fraction suggesting that this intermediate is very transitory, and may indicate the reason why there is no obvious intermediate state reflected in the equilibrium unfolding curves. In contrast, the intermediate of the ΔE155 enzymes is clearly distinguishable at lower urea concentrations and has an increased area of exposed hydrophobic surface as illustrated by the ANS binding data (Figure 4c).

Thermodynamic analysis of urea-induced unfolding.

The thermodynamic parameters for the E155 containing and E155 deletion enzymes are shown in Table 3. The three state fit of tryptophan fluorescence data, from the wild type and A140D enzymes provided a similar total free energy change of 14.4 kcal/mol and 14.3 kcal/mol respectively, which is larger than that obtained for the ΔE155 enzymes (8.6 kcal/mol and 8.7 kcal/mol for ΔE155/E208 and ΔE155/K208 respectively). Similar results were obtained from the ANS binding data. The main difference between the wild type and the ΔE155 variant occurs in the initial unfolding to the transition intermediate. Studies using intrinsic fluorescence revealed a free energy change for this first transition of around 8.5kcal/mol for the wild type compared with around 2.8 kcal/mol for the ΔE155 variant. These data suggest that the enzymes with the E155 deletion are less stable than E155 containing enzymes, and the lower stability of ΔE155 enzymes comes primarily from a propensity to enter the first transition phase.

Reversibility of unfolding

The ability of the enzymes to re-fold after urea-induced unfolding was evaluated by fluorescence recovery and the restoration of catalytic activity (Figure 6). The two methods used here to monitor the refolding gave the similar results. Refolding of the wild type E155 containing enzymes was essentially complete after 1 hour with the recovery of around 95 %. In contrast the enzymes with the E155 deletion regained only around 70 % of their original activity or fluorescence intensity over this period. The refolding curve of wild type and A140D enzymes monitored by fluorescence can be fitted to a two-phase exponential equation, which respectively gave 3.18 ± 0.57 min^{-1} and 3.34 ± 0.52 min^{-1} for k_1, and 0.22 ± 0.06 $min^{-1}$and 0.27 ± 0.05 min^{-1} for k_2 with an R^2=0.9984 and 0.9992. However, refolding of the ΔE155/K208 variant followed single-phase exponential kinetics, with a rate of 4.04 ± 0.80 min^{-1} (R^2 = 0.9978). This suggests that the ΔE155 variants still have a similar fast refolding phase like the wild type and A140D enzymes, but have lost the second slow refolding phase as shown in figure 6.

Discussion

Previous studies have indicated that the polymorphic deletion of E155 causes a deficiency of GSTO1-1 in cell lines but the mechanism causing this deficiency is not clear. As the deletion can potentially alter splicing at the end of exon 4 we previously undertook Northern blotting analysis to eliminate a splicing defect as a cause of the GSTO1-1 deficiency (Schmuck et al., 2008). That study showed that T47D breast cancer cells that are hemizygous for the E155 deletion allele produce mRNA of the appropriate size, suggesting that abnormal splicing is unlikely to be the cause of the deficiency. Previous pulse chase studies in T47D cells indicate that the E155 deletion protein has a shorter than normal $T_{1/2}$ (Schmuck et al., 2008). Although this variant can be expressed as an active enzyme in *E coli*, the recombinant enzyme is relatively heat sensitive (Schmuck et al., 2008). Given the clinical interest in GSTO1-1 we were interested to determine the mechanism by which the E155 deletion mediates this deficiency.

The crystal structure indicated that the deletion of E155 caused only small perturbations of the overall protein fold. Although there is a slight decrease in the volume and apparent accessibility of the H site, the distinct structural forms of ΔE155 dimers observed in the crystal structures point toward increased flexibility of the protein. This may explain the previously observed increase in catalytic activity of ΔE155 mutants (Table 4), as conformations suitable for binding and catalysis of diverse substrates are more accessible to the flexible mutant protein. The catalytic activity of the recombinant ΔE155 enzymes and the absence of immunologically detectable GSTO1-1 in T47D cells suggest that the deletion may cause a defect in stability or folding rather than a loss of function. We found several structural factors that could have a deleterious impact on stability including the increase in the water accessible surface area, reduction in buried hydrophobic surface area, and the large decrease in molecular contacts between helies α5 and α7. Even the increased buried area of dimer interface was not a positive factor because of the concomitant increase in the surface area of solvent exposed hydrophobic residues.

The determined free energy change $\Delta G^{0}_{N\rightarrow U}$ supports the lower stability of the ΔE155 enzymes.. We also found evidence that at low urea concentrations the ΔE155 enzymes form a transitional intermediate that is not significantly populated by the E155 containing enzymes. The unfolding intermediate formed by the ΔE155 enzymes appears to be a dimer with more hydrophobic area exposure revealed by the ANS binding data. The nature of the intermediate formed by the E155 containing enzymes is difficult to identify with the present data.

The capacity of the E155 deletion variants to refold after complete unfolding in urea was limited compared with the E155 containing A140 and D140 enzymes (figure 6). This limitation only occurred during the second slow phase of refolding. Since refolding is usually thought to be the reverse of unfolding, the refolding of the E155 deletion enzymes is probably limited by the population of the transitional intermediate. As mentioned above, the intermediate has a larger exposed hydrophobic surface, which probably promotes precipitation or prevents further refolding of the protein resulting in the lack of second slow phase for the ΔE155 enzymes. Intracellular proteins are dynamic and may be subjected to conformational changes under different intracellular conditions. It is possible that the increased accessibility to solvent and decreased contacts in the E155 deletion enzyme may promote unfolding and restrict refolding by presenting a barrier of increased hydrophobic surface exposure, leading to an dynamic equilibrium that favours an unfolded state *in vivo*.

We therefore conclude that the deletion of E155 causes GSTO1-1 deficiency by its low stability, resulting from its increased propensity to unfold, and a novel mechanism that inhibits refolding. The structural characteristics the deletion mutant, high ASA and less buried hydrophobic area and loose packing around ΔE155 agree with these observations. The results help us to understand the impact of the E155 deletion allele on the level of GSTO1-1 activity *in vivo*, which may contribute to the observed association of GSTO1 with the age at onset of Alzheimers disease and the activation of the pro-inflammatory cytokine IL1β.

Acknowledgements
This study was supported by Project Grant 366731 from the National Health and Medical Research Council. The authors would like to express their gratitude to Professor Mitchell Guss, of the School of Molecular and Microbial Biosciences, University of Sydney, for the use of equipment during X-ray data collection.

References

Adams, P. D., Grosse-Kunstleve, R. W., Hung, L. W., Ioerger, T. R., McCoy, A. J., Moriarty, N. W., Read, R. J., Sacchettini, J. C., Sauter, N. K. & Terwilliger, T. C. (2002). PHENIX: building new software for automated crystallographic structure determination. *Acta Crystallogr D Biol Crystallogr, 58*, 1948-1954.

Baker, R. T., Catanzariti, A. M., Karunasekara, Y., Soboleva, T. A., Sharwood, R., Whitney, S. & Board, P. G. (2005). Using deubiquitylating enzymes as research tools. *Methods Enzymol, 398*, 540-554.

Board, P. G. & Anders, M. W. (2007). Glutathione transferase omega 1 catalyzes the reduction of S-(phenacyl)glutathiones to acetophenones. *Chem Res Toxicol, 20*, 149-154.

Board, P. G., Coggan, M., Cappello, J., Zhou, H., Oakley, A. J. & Anders, M. W. (2008). S-(4-Nitrophenacyl)glutathione is a specific substrate for glutathione transferase omega 1-1. *Anal Biochem, 374*, 25-30.

Board, P. G., Coggan, M., Chelvanayagam, G., Easteal, S., Jermiin, L. S., Schulte, G. K., Danley, D. E., Hoth, L. R., Griffor, M. C., Kamath, A. V., Rosner, M. H., Chrunyk, B. A., Perregaux, D. E., Gabel, C. A., Geoghegan, K. F. & Pandit, J. (2000). Identification, Characterization and Crystal structure of the Omega Class Glutathione Transferases. *J Biol Chem, 275*, 24798-24806.

Davis, I. W., Leaver-Fay, A., Chen, V. B., Block, J. N., Kapral, G. J., Wang, X., Murray, L. W., Arendall, W. B., 3rd, Snoeyink, J., Richardson, J. S. & Richardson, D. C. (2007). MolProbity: all-atom contacts and structure validation for proteins and nucleic acids. *Nucleic Acids Res, 35*, W375-383.

Dulhunty, A., Gage, P., Curtis, S., Chelvanayagam, G. & Board, P. (2001). The Glutathione Transferase Structural Family Includes a Nuclear Chloride Channel and a Ryanodine Receptor Calcium Release Channel Modulator. *J Biol Chem, 276*, 3319-3323.

Emsley, P. & Cowtan, K. (2004). Coot: model-building tools for molecular graphics. *Acta Crystallogr D Biol Crystallogr, 60*, 2126-2132.

Erhardt, J. & Dirr, H. (1995). Native dimer stabilizes the subunit tertiary structure of porcine class pi glutathione S-transferase. *Eur J Biochem, 230*, 614-620.

Gloss, L. M. & Matthews, C. R. (1997). Urea and thermal equilibrium denaturation studies on the dimerization domain of Escherichia coli Trp repressor. *Biochemistry, 36*, 5612-5623.

Jones, T. A., Zou, J. Y., Cowan, S. W. & Kjeldgaard, M. (1991). Improved Methods for Building Protein Models in Electron-Density Maps and the Location of Errors in These Models. *Acta Crystallographica Section A, 47*, 110-119.

Kolsch, H., Larionov, S., Dedeck, O., Orantes, M., Birkenmeier, G., Griffin, W. S. & Thal, D. R. (2007). Association of the Glutathione S-transferase Omega-1 Ala140Asp Polymorphism With Cerebrovascular Atherosclerosis and Plaque-Associated Interleukin-1{alpha} Expression. *Stroke, 38*, 2847-2850.

Kolsch, H., Linnebank, M., Lutjohann, D., Jessen, F., Wullner, U., Harbrecht, U., Thelen, K. M., Kreis, M., Hentschel, F., Schulz, A., von Bergmann, K., Maier, W. & Heun, R. (2004). Polymorphisms in glutathione S-transferase omega-1 and AD, vascular dementia, and stroke. *Neurology, 63*, 2255-2260.

Krissinel, E. & Henrick, K. (2007). Inference of macromolecular assemblies from crystalline state. *J Mol Biol, 372*, 774-797.

Lakowicz, J. (1986). *Principles of fluorescence spectroscopy,* (Editor ed.). New York: Plenum Press.

Laliberte, R. E., Perregaux, D. G., Hoth, L. R., Rosner, P. J., Jordan, C. K., Peese, K. M., Eggler, J. F., Dombroski, M. A., Geoghegan, K. F. & Gabel, C. A. (2003). Glutathione s-transferase omega 1-1 is a target of cytokine release inhibitory drugs and may be responsible for their effect on interleukin-1beta posttranslational processing. *J Biol Chem, 278***,** 16567-16578.

Li, Y. J., Oliveira, S. A., Xu, P., Martin, E. R., Stenger, J. E., Scherzer, C. R., Hauser, M. A., Scott, W. K., Small, G. W., Nance, M. A., Watts, R. L., Hubble, J. P., Koller, W. C., Pahwa, R., Stern, M. B., Hiner, B. C., Jankovic, J., Goetz, C. G., Mastaglia, F., Middleton, L. T., Roses, A. D., Saunders, A. M., Schmechel, D. E., Gullans, S. R., Haines, J. L., Gilbert, J. R., Vance, J. M. & Pericak-Vance, M. A. (2003). Glutathione S-transferase omega-1 modifiesage-at-onset of Alzheimer disease and Parkinson disease. *Hum Mol Genet, 12***,** 3259-3267.

Li, Y. J., Scott, W. K., Hedges, D. J., Zhang, F., Gaskell, P. C., Nance, M. A., Watts, R. L., Hubble, J. P., Koller, W. C., Pahwa, R., Stern, M. B., Hiner, B. C., Jankovic, J., Allen, F. A., Jr., Goetz, C. G., Mastaglia, F., Stajich, J. M., Gibson, R. A., Middleton, L. T., Saunders, A. M., Scott, B. L., Small, G. W., Nicodemus, K. K., Reed, A. D., Schmechel, D. E., Welsh-Bohmer, K. A., Conneally, P. M., Roses, A. D., Gilbert, J. R., Vance, J. M., Haines, J. L. & Pericak-Vance, M. A. (2002). Age at onset in two common neurodegenerative diseases is genetically controlled. *Am J Hum Genet, 70***,** 985-993.

Li, Y. J., Scott, W. K., Zhang, L., Lin, P. I., Oliveira, S. A., Skelly, T., Doraiswamy, M. P., Welsh-Bohmer, K. A., Martin, E. R., Haines, J. L., Pericak-Vance, M. A. & Vance, J. M. (2006). Revealing the role of glutathione S-transferase omega in age-at-onset of Alzheimer and Parkinson diseases. *Neurobiol Aging, 27***,** 1087-1093.

Marnell, L. L., Garcia-Vargas, G. G., Chowdhury, U. K., Zakharyan, R. A., Walsh, B., Avram, M. D., Kopplin, M. J., Cebrian, M. E., Silbergeld, E. K. & Aposhian, H. V. (2003). Polymorphisms in the human monomethylarsonic acid (MMA V) reductase/hGSTO1 gene and changes in urinary arsenic profiles. *Chem Res Toxicol, 16***,** 1507-1513.

Mukherjee, B., Salavaggione, O. E., Pelleymounter, L. L., Moon, I., Eckloff, B. W., Schaid, D. J., Wieben, E. D. & Weinshilboum, R. M. (2006). Glutathione S-transferase omega 1 and omega 2 pharmacogenomics. *Drug Metab Dispos, 34***,** 1237-1246.

Murshudov, G. N., Vagin, A. A. & Dodson, E. J. (1997). Refinement of macromolecular structures by the maximum-likelihood method. *Acta Crystallographica Section D-Biological Crystallography, 53***,** 240-255.

Otwinowski, Z. & Minor, W. (1997). Processing of x-ray diffraction data colllected in oscillation mode. *Methods in Enzymology, 276***,** 307-326.

Paiva, L., Marcos, R., Creus, A., Coggan, M., Oakley, A. J. & Board, P. G. (2008). Polymorphism of glutathione transferase Omega 1 in a population exposed to a high environmental arsenic burden

. *Pharmacogenetic and Genomics, 18***,** 1-10.

Schmuck, E., Cappello, J., Coggan, M., Brew, J., Cavanaugh, J. A., Blackburn, A. C., Baker, R. T., Eyre, H. J., Sutherland, G. R. & Board, P. G. (2008). Deletion of Glu155 causes a deficiency of glutathione transferase Omega 1-1 but does not alter sensitivity to arsenic trioxide and other cytotoxic drugs. *Int J Biochem Cell Biol, 40***,** 2553-2559.

Schmuck, E. M., Board, P. G., Whitbread, A. K., Tetlow, N., Cavanaugh, J. A., Blackburn, A. C. & Masoumi, A. (2005). Characterization of the

monomethylarsonate reductase and dehydroascorbate reductase activities of Omega class glutathione transferase variants: implications for arsenic metabolism and the age-at-onset of Alzheimer's and Parkinson's diseases. *Pharmacogenet Genomics, 15*, 493-501.

Szpikowska, B. K. & Mas, M. T. (1996). Urea-induced equilibrium unfolding of single tryptophan mutants of yeast phosphoglycerate kinase: evidence for a stable intermediate. *Arch Biochem Biophys, 335*, 173-182.

Tanaka-Kagawa, T., Jinno, H., Hasegawa, T., Makino, Y., Seko, Y., Hanioka, N. & Ando, M. (2003). Functional characterization of two variant human GSTO 1-1s (Ala140Asp and Thr217Asn). *Biochem Biophys Res Commun, 301*, 516-520.

Vagin, A. A. & Teplyakov, A. (1997). MOLREP: an automated program for molecular replacement. *Journal of Applied Crystallography*, 1022-1025.

Whitbread, A. K., Masoumi, A., Tetlow, N., Schmuck, E., Coggan, M. & Board, P. G. (2005). Characterization of the omega class of glutathione transferases. *Methods Enzymol, 401*, 78-99.

Whitbread, A. K., Tetlow, N., Eyre, H. J., Sutherland, G. R. & Board, P. G. (2003). Characterization of the human Omega class glutathione transferase genes and associated polymorphisms. *Pharmacogenetics, 13*, 131-144.

Yu, L., Kalla, K., Guthrie, E., Vidrine, A. & Klimecki, W. T. (2003). Genetic variation in genes associated with arsenic metabolism: glutathione S-transferase omega 1-1 and purine nucleoside phosphorylase polymorphisms in European and indigenous Americans. *Environ Health Perspect, 111*, 1421-1427.

Zakharyan, R. A., Sampayo-Reyes, A., Healy, S. M., Tsaprailis, G., Board, P. G., Liebler, D. C. & Aposhian, H. V. (2001). Human monomethylarsonic acid (MMA(V)) reductase is a member of the glutathione-S-transferase superfamily. *Chem Res Toxicol, 14*, 1051-1057.

Table 1. X-Ray Data Collection and Refinement Statistics

Space group	$P2_12_12$
Unit-cell parameters (Å)	a = 73.0, b = 201.9, c = 53.4
Reflections measured / unique	389373 / 44498
Resolution range (Å)	36.51-2.10 (2.18-2.10†)
R-merge (%)	12.8 (37.0†)
Completeness	94.4 (80.7†)
Mean I/σI	21.4 (3.5†)
R / R_{free} (%)	19.91 / 26.05
rmsd bonds (Å)	0.008
rmsd angles (°)	1.120
PDB Accession code	3LFL

†, the highest resolution bin

Table 2. Interface and surface analysis of ΔE155/E208 and wild type crystal structure

	Solved residues	SA of dimer(Å^2)	Total buried area of dimer(Å^2)	Total SA of Trp residues in dimer(Å^2)	Buried area of dimer interface(Å^2)
GSTO1 wild type (1eem)	Ser5-Leu241	20961.5	3859.9	32.48	1885.6
ΔE155 monomer A	Ser5-Leu240	21639.1	3317.3	33.74	2116.6

All calculations come from online PISA (Krissinel and Henrick, 2007) of EBI services

Table 3. Thermodynamic parameters characterising the urea-induced unfolding transition monitored by tryptophan fluorescence and ANS binding.

	Two state fit[a]						
	$\Delta G^0_{N\rightarrow U}$(kcal/mol)	$m_{N\rightarrow U}$(kcal/mol/M)	$[urea]_{1/2}$ (M)				$\Delta G^0_{N\rightarrow U}$(kcal/mol)
Tryptophan fluorescence							
WT	6.41±0.32	1.32±0.07	4.86±0.03				6.41
A140D	5.15±0.36	1.05±0.08	4.92±0.06				5.15
ANS binding							
WT	8.21±0.71	1.59±0.14	5.17±0.04				8.21
A140D	7.78±1.06	1.47±0.20	5.30±0.07				7.78
	Three state fit[b]						
	$\Delta G^0_{N\rightarrow I}$(kcal/mol)	$m_{N\rightarrow I}$(kcal/mol/M)	$[urea]_{1/2,I}$(M)	$\Delta G^0_{I\rightarrow U}$(kcal/mol)	$m_{I\rightarrow U}$(kcal/mol/M)	$[urea]_{1/2,2}$(M)	
Tryptophan fluorescence							
WT	8.51±0.46	1.81±0.11	4.69±0.06	5.91±2.42	1.00±0.36	5.91±0.33	14.42
A140D	9.16±0.82	2.02±0.20	4.55±0.09	5.14±1.67	0.87±0.26	5.94±0.22	14.3
ΔE155/E208	2.84±0.79	1.48±0.37	1.92±0.12	5.78±0.35	1.37±0.08	4.22±0.03	8.62
ΔE155/K208	3.34±0.97	1.80±0.49	1.86±0.11	5.39±0.31	1.29±0.07	4.19±0.03	8.73
ANS binding							
WT	7.65±2.43	2.45±0.80	3.11±0.11	7.07±0.42	1.44±0.08	4.91±0.03	14.72
A140D	5.43±2.41	2.10±0.91	2.58±0.14	5.58±0.57	1.13±0.12	4.93±0.06	11.01
ΔE155/E208	3.51±1.55	1.95±0.77	1.77±0.17	6.54±0.58	1.55±0.13	4.20±0.04	10.05
ΔE155/K208	3.89±1.64	1.88±0.79	2.06±0.15	4.98±0.62	1.27±0.14	3.92±0.07	8.87

[a] fitted according to the two state model ($N_2\rightarrow 2U$). [b] fitted to the three state model via a dimeric intermediate.

Table 4. The activity of recombinant wild type and delE155 GSTO1-1 variants with a range of substrates.

Enzyme	CDNB	Thiol transferase	Dehydroascorbate	Monomethylarsonate	Dimethylarsonate	2,4-DCPG
hGSTO1-1	0.047±0.01 0.039±0.01	2±0.21 2.6±0.26	0.13±0.005	0.33±0.037	0.12±0.006	1.3±0.1
ΔE155, E208		6±0.09	0.25±0.045	0.65±0.007	0.3±0.014	1.3±0.05
ΔE155, K208	0.063±0.01	4.8±0.07 3.6±0.36	0.21±0.03	0.67±0.066	0.37±0.015	1.1±0.03

All activities shown as μmol/min/mg, mean±SD. CDNB ; 1-chloro-2,4,dinitrobenzene. 2,4-DCPG ; S-(2,4-dichlorophenacylglutathione).
All data compiled from (Board and Anders, 2007, Whitbread et al., 2003, Schmuck et al., 2005)

Figure legends

Figure 1: Structural changes induced by the deletion of E155. **(A)** A view perpendicular to the crystallographic two-fold axis of the native structure (translucent yellow), the ΔE155 A monomer (cyan) and the non-crystallographic two-fold axis of the ΔE155 B and C monomers (magenta) which produce the GSTO1-1 physiological dimer. The position of E155 and GSH are shown with stick representation. **(B)** A closer inspection of the deletion site within the ΔE155 A-monomer (cyan) compared with the wild-type enzyme (yellow). Changes to the associated residue side chain conformations in stick representation. The new interaction formed at the dimer interface is also visible. The adjacent monomer is shown in magenta. The figures were generated using PyMol (http://www.pymol.org.)

Figure 2: The flexibility of helix α9 observed in the ΔE155 structure. **(A)** A closer view of the A monomer active site reveals several key differences compared with the native enzyme. Of most interest is the different rotamer adopted by Trp222, dramatically increasing the hydrophobicity within the conserved 'H-site'. The ΔE155 A-monomer is shown in cyan compared with the wild-type enzyme in yellow. **(B)** Comparison of the native structure to that of the B monomer reveals much more pronounced structural change. Helix α9 has shifted towards the site of glutathione binding by several Angstroms, dramatically reducing the size of the 'H-site'. The ΔE155 B-monomer is shown in magenta with the overlayed native structure in yellow. The figures were generated using PyMol (http://www.pymol.org.)

Figure 3. Tryptophan fluorescence quenching by acrylamide. The experimental values and trend lines are shown as (●) wild type, (○) A140D, (▼) ΔE155/E208, and (△) ΔE155/K208.

Figure 4. The equilibrium unfolding of GSTO1-1 in urea. Unfolding was monitored by (a) tryptophan fluorescence expressed as the ratio of fluorescence at 333nm to the fluorescence at 355nm, (b) ellipticity at 222nm of circular dichroism, and (c) relative intensity of ANS binding. The three state curve fits of $N_2 \leftrightarrow I \leftrightarrow 2U$ are shown in (a) and (c). The inset in (a) is the 2-state fitting result for wild type and A140D, which is less consistent with the experimental values at high urea concentration compared with the 3-state fit. The calculated population of the native, intermediate, and unfolded states of GSTO1-1 as a function of urea concentration are plotted for wild type and A140D (d, solid line for wild type and dashed line for A140D), ΔE155/E208 (e), and ΔE155/K208 (f). The experimental values for each enzyme are shown as (●) wild type, (○) A140D, (▼) ΔE155/E208, and (△) ΔE155/K208.

Figure 5. The protein concentration dependence of equilibrium unfolding of GSTO1-1 variants in urea. The unfilled symbols represent determinations at 1μM protein and the filled symbols represent determinations at 8μM protein.

Figure 6. Refolding of GSTO1 variants. Symbols and solid curves represent the recovery of fluorescence. The right-hand columns show the recovery of activity with 4-NPG as a substrate (mean + SD).

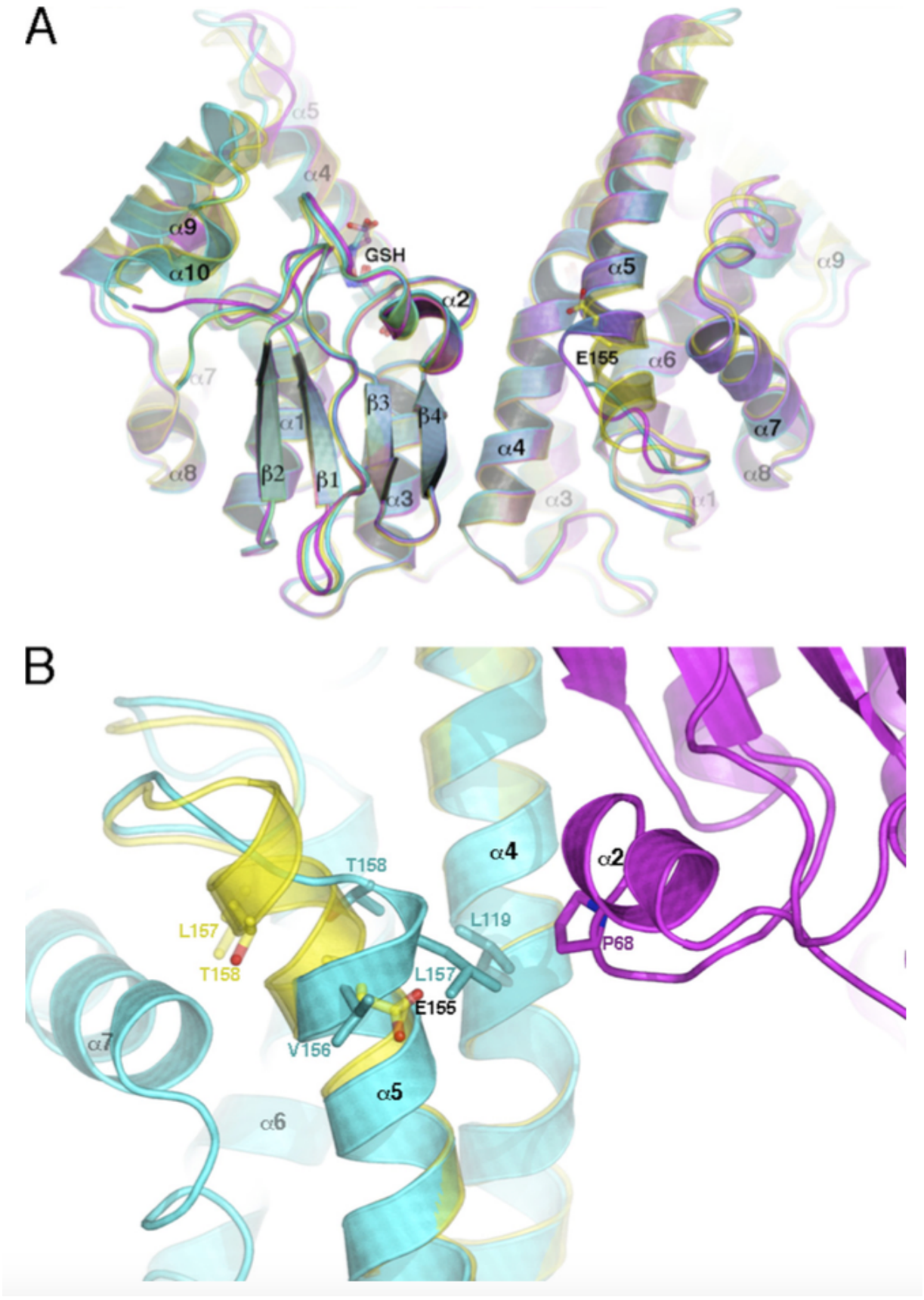
A
α5
α4
α9
α10
GSH
α2
α7
β3
α1
β4
α4
β2
β1
α8
α3
α5
E155
α6
α9
α7
α8
α3
α1
B
T158
α4
α2
L157
L119
P68
T158
L157
E155
α7
V156
α5
α6

Figure 1

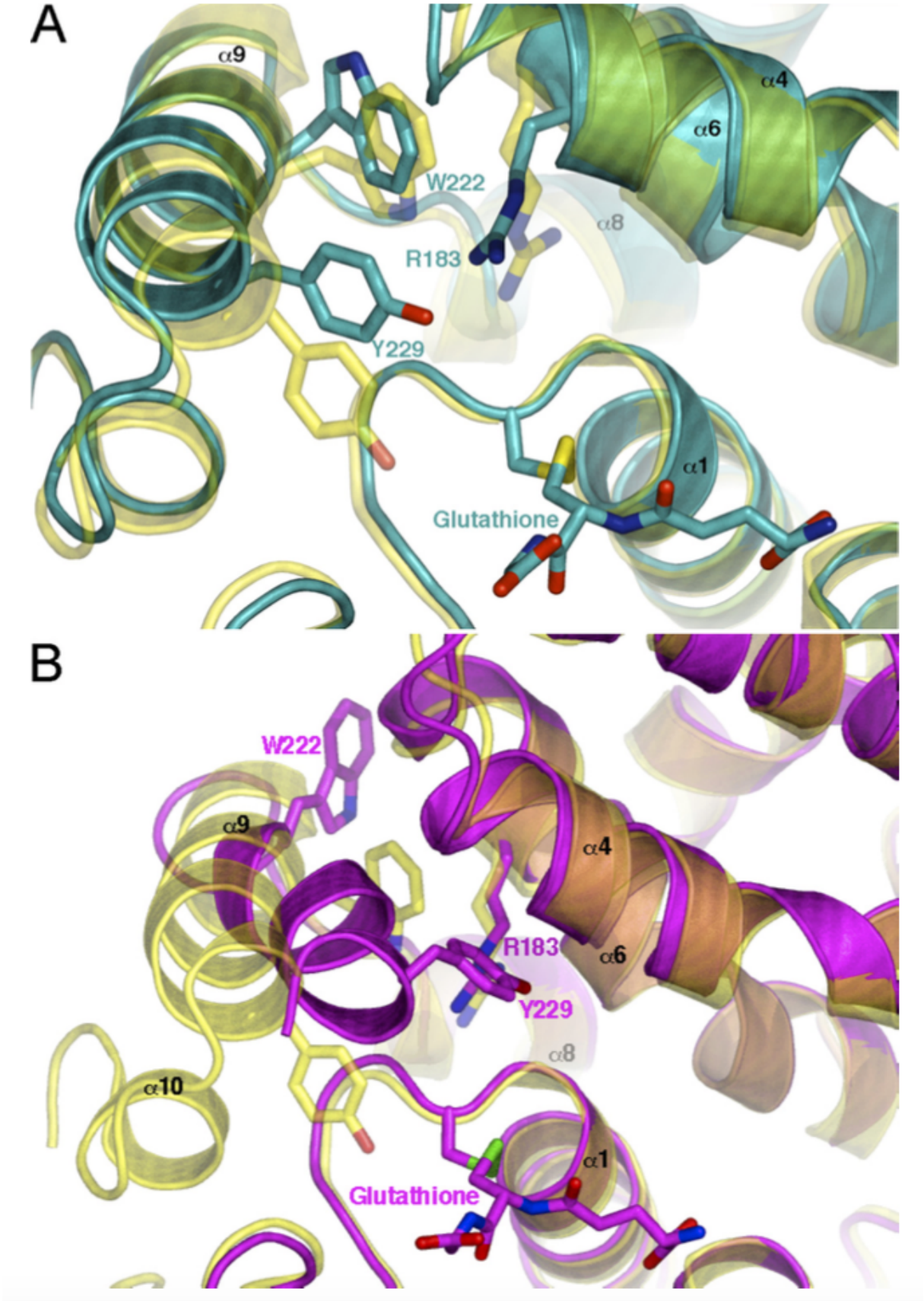
A
α9
α4
α6
W222
α8
R183
Y229
α1
Glutathione
B
W222
α9
α4
R183
α6
Y229
α8
α10
α1
Glutathione

Figure 2

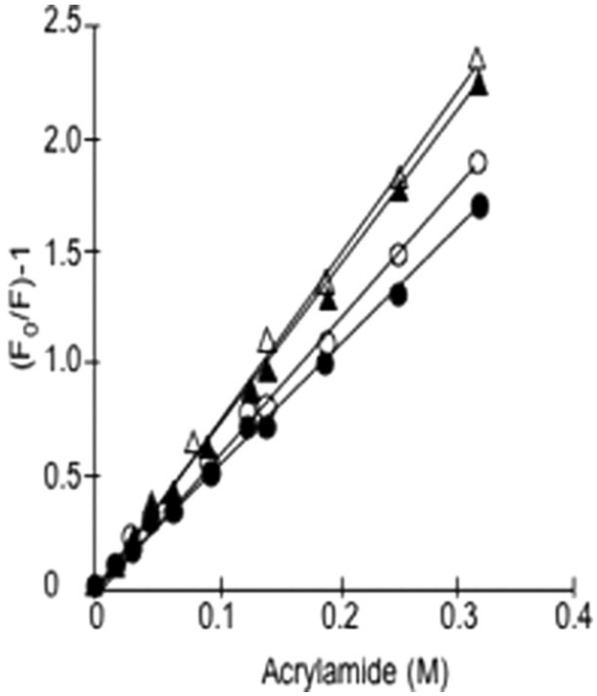

Figure 3

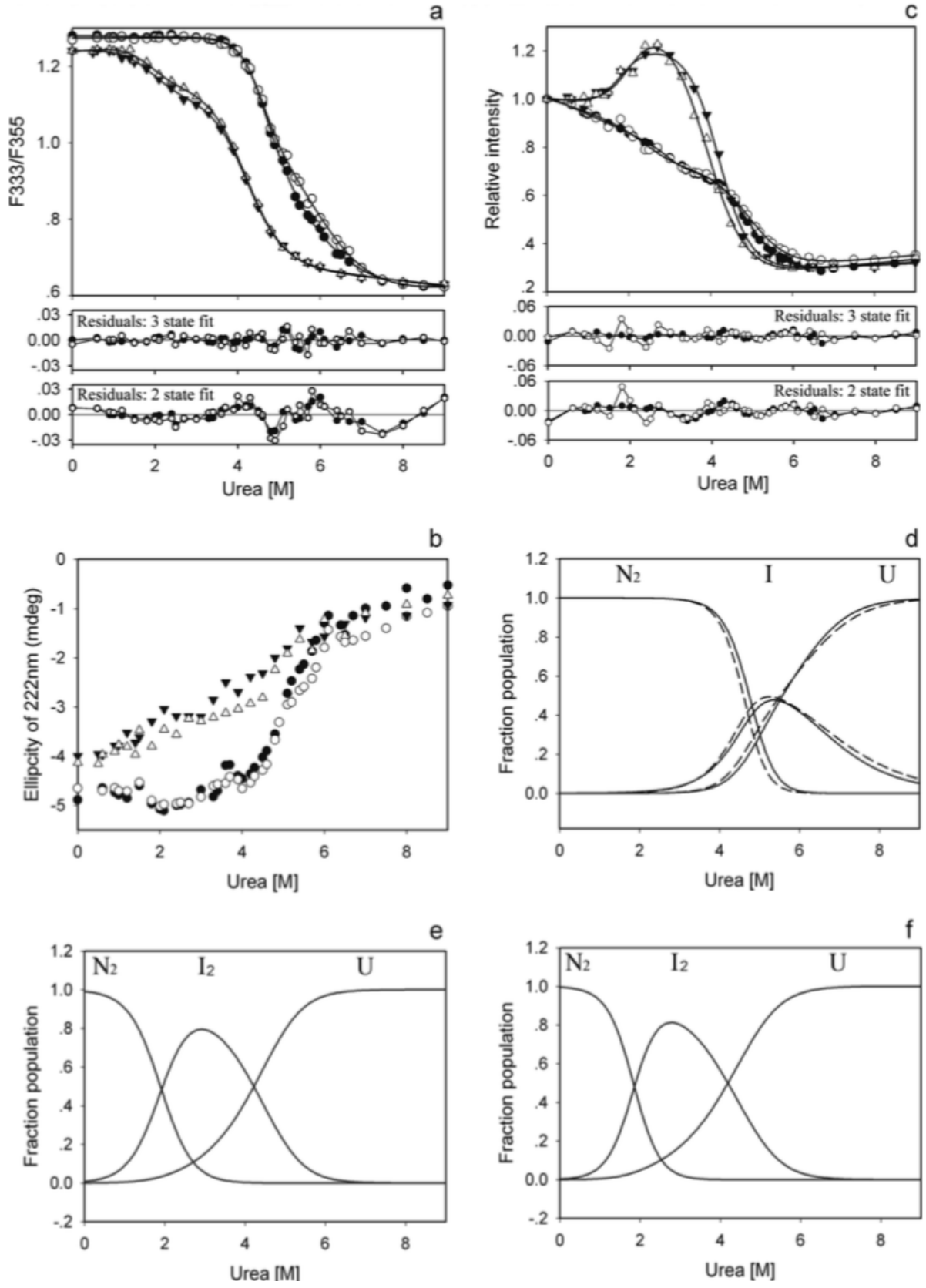
a
F333/F355
Residuals: 3 state fit
Residuals: 2 state fit
Urea [M]
c
Relative intensity
Residuals: 3 state fit
Residuals: 2 state fit
Urea [M]
b
Ellipcity of 222nm (mdeg)
Urea [M]
d
N2
I
U
Fraction population
Urea [M]
e
N2
I2
U
Fraction population
Urea [M]
f
N2
I2
U
Fraction population
Urea [M]

Figure 4

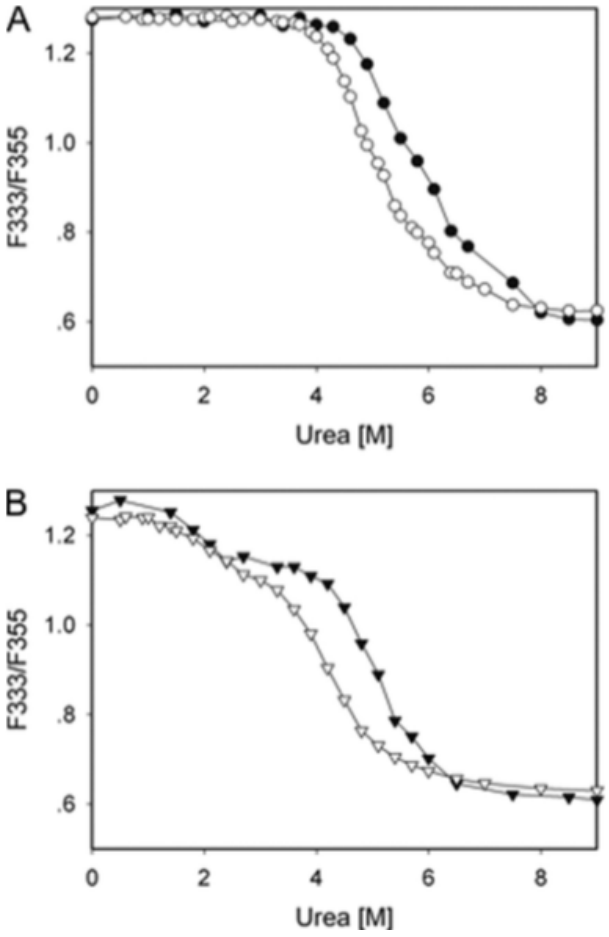
A
1.2
1.0
.8
.6
F333/F355
0
2
4
6
8
Urea [M]
B
1.2
1.0
.8
.6
F333/F355
0
2
4
6
8
Urea [M]

Figure 5

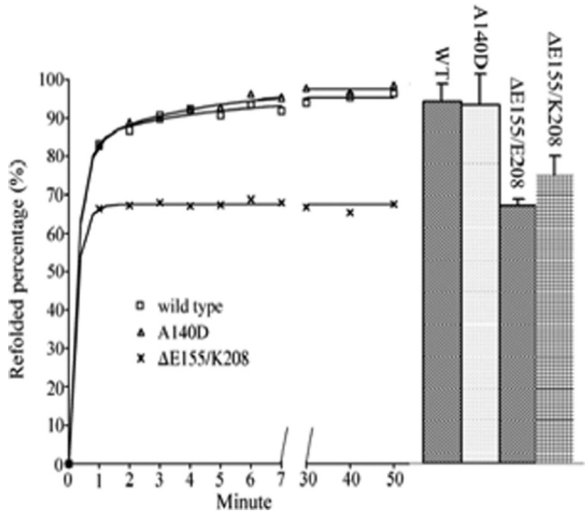
Refolded percentage (%)
100
90
80
70
60
50
40
30
20
10
0
wild type
A140D
ΔE155/K208
0 1 2 3 4 5 6 7 30 40 50
Minute
WT
A140D
ΔE155/E208
ΔE155/K208

Figure 6